# Peroxisome Proliferator Activated Receptor Gamma Controls Mature Brown Adipocyte Inducibility through Glycerol Kinase

Lasar, David ; Rosenwald, Matthias ; Kiehlmann, Elke ; Balaz, Miroslav ; Tall, Bettina ; Opitz, Lennart ; Lidell, Martin E ; Zamboni, Nicola ; Krznar, Petra ; Sun, Wenfei ; Varga, Lukas ; Stefanicka, Patrik ; Ukropec, Jozef ; Nuutila, Pirjo ; Virtanen, Kirsi ; Amri, Ez-Zoubir ; Enerbäck, Sven ; Wahli, Walter ; Wolfrum, Christian

Abstract: Peroxisome proliferator-activated receptors (PPARs) have been suggested as the master regulators of adipose tissue formation. However, their role in regulating brown fat functionality has not been resolved. To address this question, we generated mice with inducible brown fat-specific deletions of PPAR , / , and , respectively. We found that both PPAR and / are dispensable for brown fat function. In contrast, we could show that ablation of PPAR in vitro and in vivo led to a reduced thermogenic capacity accompanied by a loss of inducibility by -adrenergic signaling, as well as a shift from oxidative fatty acid metabolism to glucose utilization. We identified glycerol kinase (Gyk) as a partial mediator of PPAR function and could show that Gyk expression correlates with brown fat thermogenic capacity in human brown fat biopsies. Thus, Gyk might constitute the link between PPAR -mediated regulation of brown fat function and activation by -adrenergic signaling.

DOI: https://doi.org/10.1016/j.celrep.2017.12.067

Article

Cell Reports

# Peroxisome Proliferator Activated Receptor Gamma Controls Mature Brown Adipocyte Inducibility through Glycerol Kinase

## Graphical Abstract

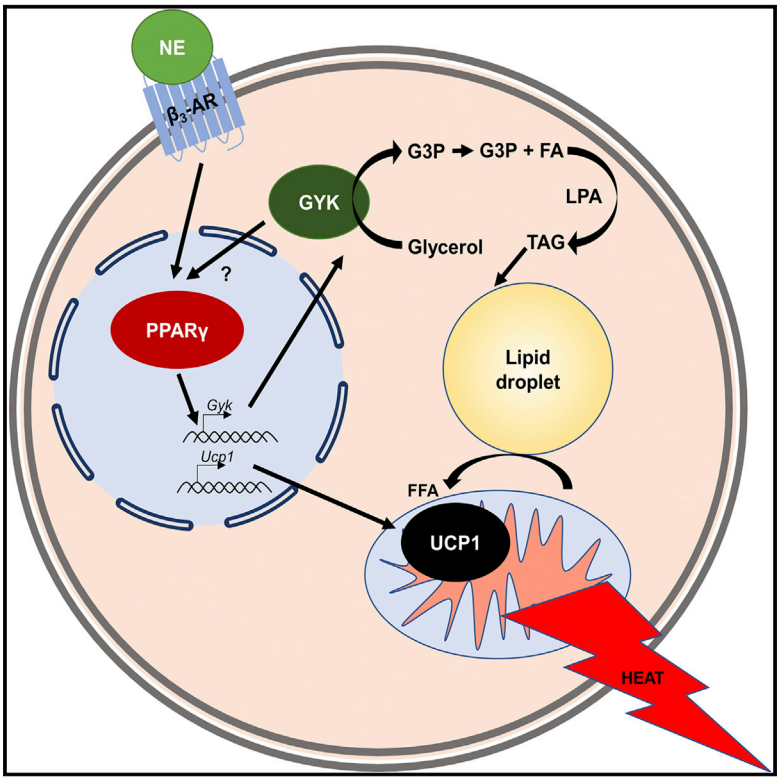


## Authors

David Lasar, Matthias Rosenwald, Elke Kiehlmann, ..., Sven Enerbäck, Walter Wahli, Christian Wolfrum

## Correspondence

christian-wolfrum@ethz.ch

## In Brief

Lasar et al. show that PPARγ is required to maintain the thermogenic capacity of mature brown adipocytes, which can be induced by activating β-adrenergic signaling. They show that expression of the known PPARγ target Gyk correlates with human brown fat activity and identify Gyk as a partial mediator of PPARγ function.

## Highlights

- PPARα and β/δ are dispensable for maintaining brown adipocyte function *in vivo*
- PPARγ is needed for β-adrenergic signaling-mediated induction of brown adipocytes
- Gyk, a known target of PPARγ, is a partial mediator of the effects of PPARγ
- Loss of Gyk leads to regulation of PPARγ target genes by an unknown mechanism

## Data and Software Availability

GSE103474

Lasar et al., 2018, Cell Reports *22*, 760–773
January 16, 2018 
https://doi.org/10.1016/j.celrep.2017.12.067

CellPress

OPEN ACCESS
CellPress

Cell Reports
Article

# Peroxisome Proliferator Activated Receptor Gamma Controls Mature Brown Adipocyte Inducibility through Glycerol Kinase

David Lasar,[1] Matthias Rosenwald,[1] Elke Kiehlmann,[1] Miroslav Balaz,[1] Bettina Tall,[1] Lennart Opitz,[8] Martin E. Lidell,[3] Nicola Zamboni,[2] Petra Krznar,[2] Wenfei Sun,[1] Lukas Varga,[10] Patrik Stefanicka,[10] Jozef Ukropec,[9] Pirjo Nuutila,[11,12] Kirsi Virtanen,[11,12] Ez-Zoubir Amri,[5,6,7] Sven Enerbäck,[3] Walter Wahli,[4] and Christian Wolfrum[1,13,*]

[1]Institute of Food, Nutrition and Health, ETH Zurich, Schorenstrasse 16, 8603 Schwerzenbach, Switzerland
[2]Department of Biology, Institute for Molecular Systems Biology, Eidgenössische Technische Hochschule Zürich, 8093 Zurich, Switzerland
[3]Department of Medical and Clinical Genetics, Institute of Biomedicine, The Sahlgrenska Academy, University of Gothenburg, Gothenburg 405 30, Sweden
[4]Lee Kong Chian School of Medicine, Nanyang Technological University, Singapore 308232, Singapore Center for Integrative Genomics, University of Lausanne, 1015 Lausanne, Switzerland
[5]University Nice Sophia Antipolis, iBV, UMR 7277 Nice, France
[6]CNRS, iBV UMR 7277 Nice, France
[7]Inserm, iBV, U1091 Nice, France
[8]Functional Genomics Center Zurich, ETH Zurich/University of Zurich, Winterthurerstrasse 190, 8057 Zurich, Switzerland
[9]Institute of Experimental Endocrinology, Biomedical Research Center at the Slovak Academy of Sciences, 84505 Bratislava, Slovakia
[10]Department of Otorhinolaryngology – Head and Neck Surgery, Faculty of Medicine and University Hospital, Comenius University, 81499 Bratislava, Slovakia
[11]Turku PET Centre, University of Turku, 20500 Turku, Finland
[12]Turku University Hospital, 20500 Turku, Finland
[13]Lead Contact
*Correspondence: christian-wolfrum@ethz.ch
https://doi.org/10.1016/j.celrep.2017.12.067

## SUMMARY

**Peroxisome proliferator-activated receptors (PPARs) have been suggested as the master regulators of adipose tissue formation. However, their role in regulating brown fat functionality has not been resolved. To address this question, we generated mice with inducible brown fat-specific deletions of PPARα, β/δ, and γ, respectively. We found that both PPARα and β/δδ are dispensable for brown fat function. In contrast, we could show that ablation of PPARγ *in vitro* and *in vivo* led to a reduced thermogenic capacity accompanied by a loss of inducibility by β-adrenergic signaling, as well as a shift from oxidative fatty acid metabolism to glucose utilization. We identified glycerol kinase (Gyk) as a partial mediator of PPARγ function and could show that Gyk expression correlates with brown fat thermogenic capacity in human brown fat biopsies. Thus, Gyk might constitute the link between PPARγ-mediated regulation of brown fat function and activation by β-adrenergic signaling.**

## INTRODUCTION

Obesity is defined as abnormal fat accumulation and occurs due to a long-term positive energy balance (Mittendorfer, 2011). The global increase in obesity has been attributed to numerous factors including, but not limited to, altered food consumption as well as a decrease in energy expenditure (Hill et al., 2012). One possibility to induce energy expenditure is non-shivering thermogenesis in brown adipose tissue (BAT). This process is mediated by Uncoupling protein 1 (UCP1), which differentiates BAT from classical white adipose tissue (WAT). Studies on the regulation of BAT function have led to the identification of key regulatory factors such as peroxisome proliferator-activated receptor γ (PPARγ), PGC1α, and PRDM16 (Ohno et al., 2012; Petrovic et al., 2010). Particularly, PPARγ2 is an important regulator of both brown and white adipocyte differentiation (Barak et al., 1999; Tontonoz et al., 1994). Recent evidence derived from the analysis of post-translational modifications of PPARγ have implicated this factor not only as a regulator of adipocyte formation, but also as a mediator of brown adipocyte functionality (Choi et al., 2010; Hu et al., 1996; Qiang et al., 2012). Furthermore, it was reported that *Ucp1* mRNA abundance is higher in animals treated with the PPARγ agonist rosiglitazone (Festuccia et al., 2010); however, whether this is due to a direct induction in mature cells or due to de novo formation of brown adipocytes is unknown. In human multipotent adipose-derived stem (hMADS) cells, rosiglitazone-induced browning leads to increased mitochondrial oxidative capacity, which is maintained independently of rosiglitazone (Loft et al., 2015). *In vivo* studies are complicated by the fact that global deletion of PPARγ leads to postnatal death at E10 (Barak et al., 1999). Thus, heterozygous PPARγ-deficient mice were shown to be protected from age-induced insulin resistance, while studies using the aP2-Cre to elicit an adipose tissue-specific knockout under obesogenic conditions showed a reduction in weight gain and

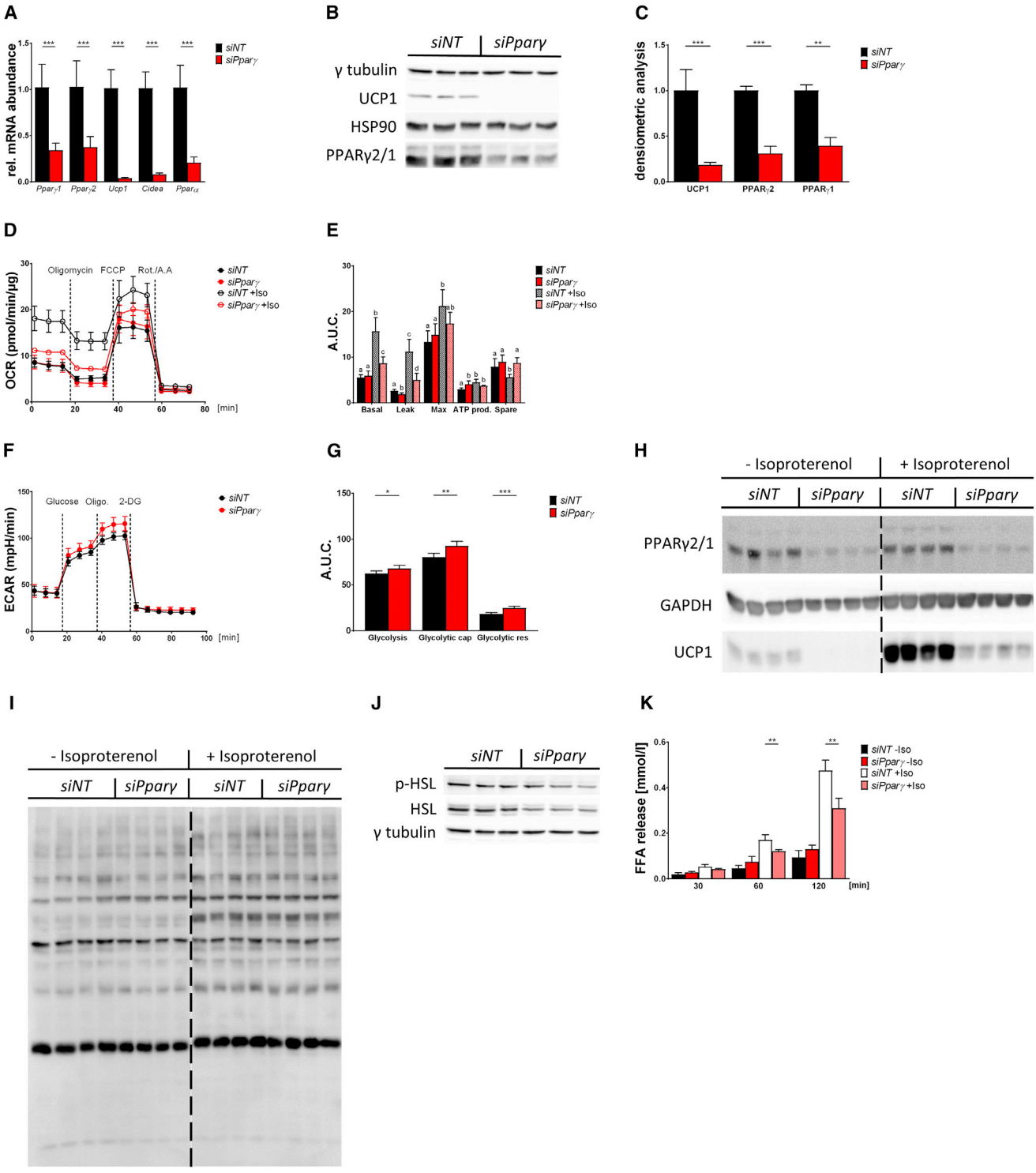


**Figure 1. Loss of PPARγ in IBA Reduces Brown-Adipocyte-Specific Marker Gene Expression and Leads to a Loss of Inducibility**

(A) mRNA abundance of reverse transfected IBA with either non-targeting (*siNT*) or *Pparγ* targeting (*siPparγ*) siRNA showing *Pparγ1*, *Pparγ2*, *Ucp1*, *Cidea*, and *Pparα* normalized to *36B4* (n = 4 per group; throughout, mRNA data are normalized to 36B4 and are expressed as mean ± SD; ***p < 0.001).

(B) Immunoblot of UCP1 and PPARγ2 and 1 in IBA transfected with *siNT* or *siPparγ*.

(C) Densiometric analysis of immunoblot (n = 3–4 per group; data are expressed as mean ± SD; **p ≤ 0.01; ***p ≤ 0.005).

(D) Mitochondrial stress test, showing OCR of IBA pre-treated with or without isoproterenol 1 hr (1 µM) before measurement (OCR-Data normalized to protein content per well; n = 5).

*(legend continued on next page)*

lipodystrophy (He et al., 2003; Jones et al., 2005). Interestingly, a murine study using the aP2-CRE-ER$^{T2}$ driver line to promote a tamoxifen-dependent inducible knockout of PPARγ demonstrated a reduction of white and brown adipocyte survival (Imai et al., 2004); however, given the drastic metabolic phenotype of these animals, due to ablation of PPARγ in white adipocytes, it is unclear to what extent PPARγ expression in BAT contributes to the observed phenotype. While it is well accepted that PPARγ at least in part mediates mature brown adipocyte functionality, surprisingly little data exist on downstream targets. It has been previously shown that PPARγ activates UCP1 expression by binding to the *UCP1* peroxisome proliferator response element (PPRE) by nuclear translocation and binding of factors like retinoid X receptor (RXR) and PGC1α (Cao et al., 2004).

Here, we demonstrate that PPARγ maintains thermogenic function and the ability of BAT to be activated by $\beta_3$-stimulation. Using transcriptional analysis and loss- and gain-of-function studies, we show that part of the effect of PPARγ might be mediated through the PPARγ target glycerol kinase (GYK) (Barquissau et al., 2016; Chakrabarty et al., 1983; Guan et al., 2002; Mazzucotelli et al., 2007).

## RESULTS

To analyze the role of PPARγ in mature brown adipocytes and to exclude the regulation of adipocyte differentiation, we utilized a reverse transfection approach in fully differentiated, immortalized brown adipocytes (IBAs). We obtained approximately 70% of knockdown for both *Pparγ1* and *Pparγ2* on both protein and mRNA abundance (Figures 1A–1C), which led to a reduction of brown adipocyte-specific transcripts such as *Ucp1* and *Cidea* as well as *Pparα* (Figure 1A). Similarly, we could show that loss of PPARγ expression led to an almost complete loss of UCP1 protein expression (Figures 1B and 1C). To elucidate whether this effect was due to de-differentiation of the adipocytes, we analyzed gene expression of brown and white mature and precursor markers. As shown in Figure S1A, we observed a varied response; for example, the expression of the preadipocyte marker *Pref1* was reduced, suggesting that knockdown of *Pparγ* does not lead to a dedifferentiation of the mature adipocytes. In a mitochondrial stress test, basal respiration of IBAs upon PPARγ ablation was not altered; however, loss of PPARγ inhibited the ability of IBAs to respond to β-adrenergic stimulation as a result of reduced basal and leak respiration (Figures 1D and 1E). A glucose stress test demonstrated that IBAs, upon PPARγ ablation, induced glycolysis as well as the glycolytic capacity (Figures 1F and 1G). In line with these findings, we could show that induction of UCP1 protein and mRNA expression in response to a β-adrenergic stimulation was lost in IBAs with suppressed PPARγ expression (Figures 1H and S1B). The effect was independent of global PKA activity (Figure 1I) and a more detailed analysis of specific targets revealed that phosphorylated hormone sensitive lipase (pHSL) and HSL were mildly reduced after PPARγ ablation (Figure 1J). Furthermore, we observed a significant reduction of activated cAMP response element-binding protein (p-CREB) and an inability of cAMP to stimulate *Ucp1* mRNA expression in the absence of PPARγ (Figures S1C–S1E). Similarly, we could show, that PPARγ ablation led to a reduction in isoproterenol stimulated lipolysis (Figures 1K and S1F). Taken together, these findings demonstrate that loss of PPARγ in mature brown adipocytes reduces the capacity to initiate the thermogenic program by β-adrenergic stimulation.

Since no functional studies analyzing the role of PPARγ in mature brown adipocytes exist, we generated an inducible brown-fat-specific PPARγ-deficient mouse model to deplete PPARγ exclusively in mature brown adipocytes (PPARγ-BATKO). Induced genetic ablation of PPARγ led to a reduction in *Pparγ* mRNA expression (Figures 2A), a down-regulation of *Ucp1* mRNA and protein expression (Figures 2C and 2B) and of other BAT markers such as *Cidea* and *Cox7a1* (Figure 2C) and *Pparα*. Conversely, we did not observe any reduction of either *Pparγ* or *Ucp1* mRNA in iWAT (Figure S2E). Phenotypic characterization of PPARγ-BATKO mice showed neither a weight phenotype nor any differences in body composition (Figures 2D and S2A); however, we observed increased circulating TAG, cholesterol, glucose, and non-esterified fatty acids (NEFA) levels (Figures 2E–2G). PPARγ-BATKO animals had reduced BAT wet weight (Figure 2J) and histological analysis of interscapular BAT depots revealed smaller adipocytes containing less and/or smaller lipid droplets resulting in a higher cell density (Figures 2H and 2I), without any changes in total cell numbers. Last, pHSL, HSL, and the pHSL/HSL ratio were reduced in BAT of PPARγ-BATKO mice (Figures 2K and 2L). Taken together, we could show that loss of PPARγ in mature brown adipocytes leads to a reduced systemic substrate utilization, concomitant with a reduction in BAT marker gene expression.

To investigate, whether PPARγ ablation in BAT would alter systemic respiration, PPARγ-BATKO and littermate controls were cold challenged for 7 days at 8°C. Food and water intake at room temperature was similar (Figure S3A), and, while in cold, PPARγ-BATKO mice exhibited elevated food and water intake (Figure S3B). Even though core body temperature was unaffected after a prolonged cold stimulus in these mice (Figure S2D), visual examination of the mice suggested an increased shivering response, which together with alterations in food and

(E) Quantification of mitochondrial stress test (n = 5; data are expressed as mean ± SD; a, b, c, d $\leq$0.05).
(F) Glucose stress test, showing OCR of IBA (n = 5).
(G) Quantification of glucose stress test (n = 5; data are expressed as mean ± SD; *p $\leq$ 0.05; **p $\leq$ 0.01; ***p $\leq$ 0.005).
(H) Immunoblot of reverse transfected IBA with siNT or siPpar$\gamma$ pre-treated 24 hr with or without isoproterenol (1 μM) showing PPARγ2 and 1 and UCP1 expression (n = 4).
(I) Immunoblot of phospho-PKA substrate in reverse transfected IBA with siNT or siPpar$\gamma$ pre-treated 24 hr with or without isoproterenol (1 μM) (n = 4).
(J) Immunoblot of reverse transfected IBA with siNT or siPpar$\gamma$ showing phosphor-HSL and gamma tubulin (n = 3).
(K) Free fatty acid (FFA) FFA release of IBA siNT and siPPARγ treated at depicted time points, with or without isoproterenol (1 μM) pre-stimulation (n = 4; data are expressed as mean ± SD; **p $\leq$ 0.01).

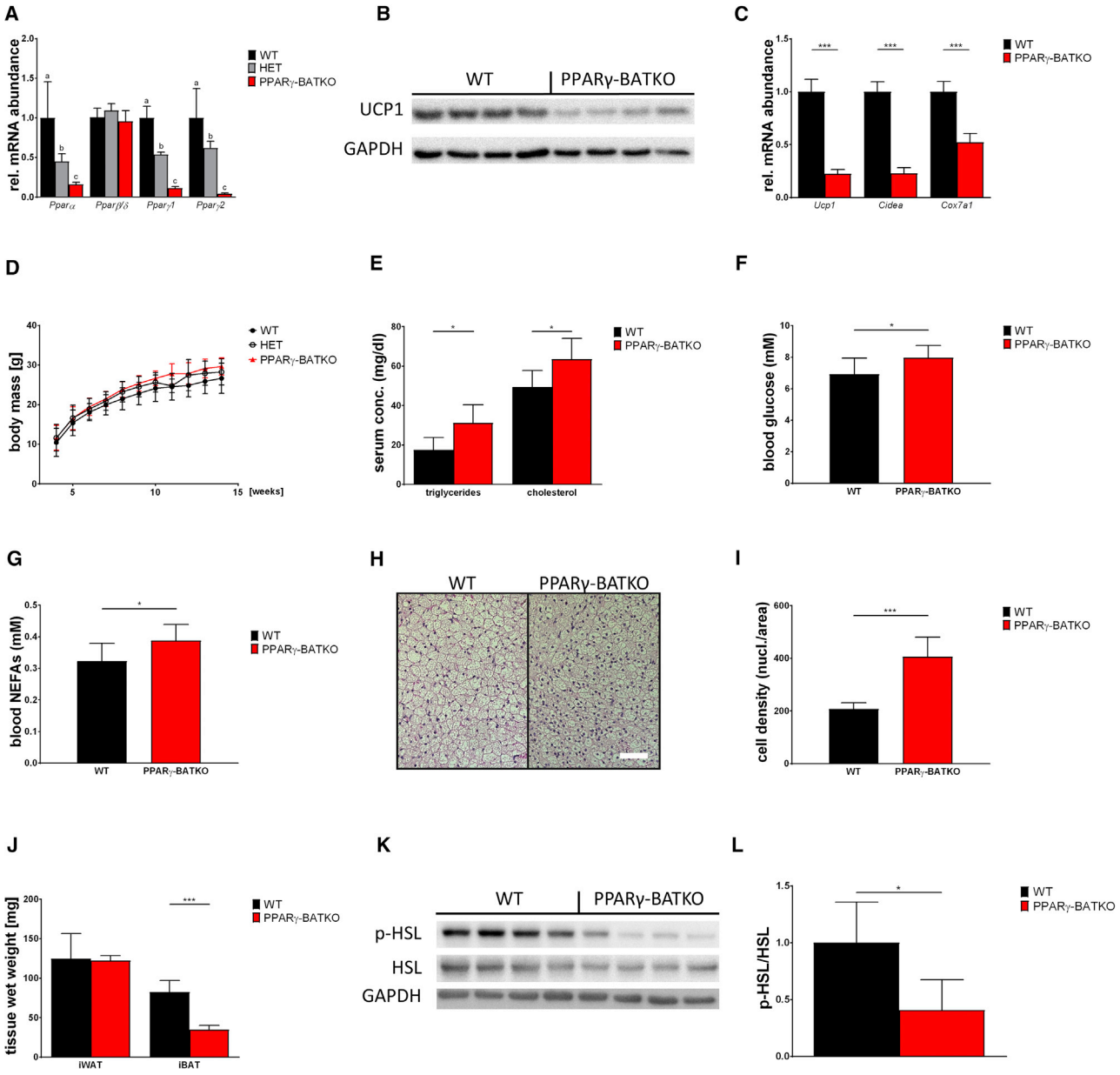


**Figure 2. Loss of PPARγ *In Vivo* Reduces BAT Size and Thermogenic Gene Expression**

(A) mRNA abundance of *Pparα*, *Pparβ/δ*, *Pparγ1*, and *Pparγ2* normalized to *36B4* in BAT of WT, HET, and PPARγ-BATKO animals (n = 6 WT versus 8 HET versus 8 PPARγ-BATKO; data are expressed as mean ± SD; a, b, c ≤ 0.05).

(B) Immunoblot of UCP1 in PPARγ-BATKO and WT animals and its respective densiometric quantification (n = 5 WT versus 4 PPARγ-BATKO).

(C) mRNA abundance of brown fat marker genes *Ucp1*, *Cidea*, and *Cox7a1* normalized to *36B4* (n = 6 WT versus 6 PPARγ-BATKO; data are expressed as mean ± SD; ***p ≤ 0.005).

(D) Body mass development of PPARγ-BATKO animals compared to Cre negative (WT) and Cre positive heterozygous littermates (HET) (n = 6 WT versus 8 HET versus 10 PPARγ-BATKO).

(E) Blood triglyceride and cholesterol of WT and PPARγ-BATKO (n = 6 WT versus 8 PPARγ-BATKO; data are expressed as mean ± SD; *p ≤ 0.05).

(F) Blood glucose levels of WT and PPARγ-BATKO (n = 6 WT versus 8 PPARγ-BATKO; data are expressed as mean ± SD; *p ≤ 0.05).

(G) Blood NEFA levels of WT and PPARγ-BATKO (n = 6 WT versus 8 PPARγ-BATKO).

(H and I) Cell density measurement of H&E-stained BAT paraffin sections (representative H&E stained BAT sections, H, and quantification, I) (n = 6 WT versus 8 PPARγ-BATKO; white scale bar, 100 μM).

(J) Tissue wet weight of WT and PPARγ-BATKO (n = 5 WT versus 4 PPARγ-BATKO; data are expressed as mean ± SD; ***p ≤ 0.005).

(K) Immunoblot of lipolytic marker HSL and its phosphorylated form (n = 5 WT versus 4 PPARγ-BATKO; data are expressed as mean ± SD; ***p ≤ 0.005).

(L) Densiometric analysis of phosphorylated and unphosphorylated HSL of WT and PPARγ-BATKO animals (n = 5 WT versus 4 PPARγ-BATKO; data are expressed as mean ± SD; *p ≤ 0.05).

water intake complicates the quantification of the contribution of PPARγ to energy expenditure (Figures S3C and S3D). Furthermore, the inability of the PPARγ-BATKO mice to induce BAT activity might affect the shivering response (Shefer and Talan, 1998), which in turn could confound the quantification of energy expenditure. Therefore, we acutely treated PPARγ-BATKO with the $\beta_3$-adrenergic receptor agonist CL316,243. Both PPARγ-BATKO and wild type mice showed similar rates of $VO_2$ and $VCO_2$ at baseline (Figures 3A and 3B). Upon CL316,243 injection, PPARγ-BATKO failed to induce respiration in the same manner as wild-type (WT) animals (Figures 3D and 3E). This reduced response in PPARγ-BATKO resulted in a higher RER in PPARγ-BATKO (Figure 3C). To exclude any compensatory effects, we repeated the experiments at thermoneutrality, which led to similar results (Figures 3D–3F). Taken together, those data underline the importance of PPARγ in maintaining brown adipocyte functionality in response to $\beta_3$-adrenergic receptor activation.

Based on previous work, we hypothesized that PPARγ controls BAT functionality by regulating *Pparα* expression (Barbera et al., 2001). In accordance, we could show that depleting PPARα in mature IBAs by reverse transfection reduced expression of brown adipocyte markers *Ucp1* and *Cidea* both on mRNA and on protein level (Figures 4A and 4B). To determine whether PPARα was also responsible for maintaining BAT function *in vivo*, we ablated PPARα specifically in BAT (PPARα-BATKO). PPARα depletion in BAT did not affect classic BAT marker expression, while bona fide PPARα markers were reduced (Figures 4C and 4D). Food and water intake were unaltered at room temperature and during cold exposure (Figure 4E) in PPARα-BATKO mice and we did not observe any changes in $VO_2$, $VCO_2$, or RER (Figures 4F–4H). Similar to PPARα, expression of *Pparβ/δ* was dispensable for BAT function, in vivo as demonstrated by the generation of PPARβ/δ-BATKO (Figures S4A and S4B). Based on these data, we conclude that PPARα plays a role in brown adipocyte function *in vitro*; however, both PPARα and PPARβ/δ seem to be dispensable for mature brown adipocyte functionality, *in vivo*.

To elucidate the pathway by which PPARγ reduces the capacity of BAT to be activated, we transcriptionally profiled the BAT of 3 days cold-challenged C57BL6/N animals and littermates at room temperature (RT), as well as IBAs in the presence or absence of PPARγ. To identify direct brown adipocyte targets of PPARγ, we analyzed both the *in vivo* and *in vitro* comparison for genes that bear PPRE, based on a published chromatin immunoprecipitation (ChIP)-atlas (Nielsen et al., 2008). We found 231 regulated genes in PPARγ-depleted IBAs and 168 genes in cold-acclimatized mice (Figure 5A). An intersection of those two lists resulted in 18 genes that were regulated *in vitro* and *in vivo* and are classified as PPAR target genes (Table S1). Of these 18 genes, only *Fabp3* and *Gyk*, which has been previously identified as a PPARγ target in BAT (Guan et al., 2005), were enriched in BAT. PPARγ knockdown in IBAs led to a significant downregulation of *Gyk* mRNA and protein expression both in the basal as well as in the isoproterenol-induced state (Figures 5B, 5C, and S5). In accordance with previous results (Festuccia et al., 2010; Festuccia et al., 2003), we could show that *Gyk* expression is elevated both in iBAT and iWAT after cold acclimatization (Table S1; Figure 5D). Additionally, we observed an increased *GYK* mRNA abundance in brown versus white differentiated hMADs cells (Figure 5E). In human deep-neck biopsies, the abundance of *GYK* correlated with *UCP1*, demonstrating that *GYK* is a surrogate for BAT quantity and activity (Figure 5F). Furthermore, positron emission tomography/computed tomography (PET/CT)-guided biopsy of human supraclavicular BAT showed higher brown adipocyte marker and *GYK* gene expression compared to WAT samples (Figure 5G). Taken together, these results confirm that GYK is a direct target of PPARγ in brown adipocytes and that similar to UCP1 GYK is regulated by cold induction in both mice and humans.

To test whether GYK ablation would result in a similar phenotype as a PPARγ knockdown, we performed a small interfering RNA (siRNA)-mediated knockdown of GYK in IBAs, which resulted in an 80% reduction of *Gyk* mRNA and protein expression (Figures 6A, 6B, and S6C). Interestingly, GYK knockdown led to a reduction of UCP1 protein expression (Figures 6B and S6D) and pHSL levels under basal and stimulated conditions. After GYK knockdown, isoproterenol treatment failed to induce both GYK and UCP1 protein expression (Figures 6C, S6C, and S6D), while we observed a slight induction of PPARγ2 but not PPARγ1 expression (Figures 6C, S6A, and S6B). GYK knockdown did change adipocyte differentiation (Figures S6G–S6I), and we were able to show that treatment of IBAs with a competitive inhibitor of GYK (Seltzer et al., 1986) led to a dose-dependent reduction in *Ucp1* levels (Figure 6D). Rosiglitazone was unable to rescue BAT-specific gene expression in GYK-ablated cells (Figure 6E), underscoring the importance of GYK for maintaining mature brown adipocyte functionality. Since GYK ablation *in vivo* causes lethality at P4 (Rahib et al., 2007), we analyzed the role of GYK in BAT by local overexpression of *Gyk* through adenoviral-mediated gene delivery in both WT and PPARγ-BATKO mice. Re-expression of GYK did not alter body weight and led to an approximately 2-fold induction of GYK expression in iBAT of both WT and PPARγ-BATKO mice (Figures 6E and 6F), which is similar to the effect of a cold stimulation. Similarly, we observed a 1.6-fold increase in iBAT weight and 2.5-fold increase in total protein mass when GYK expression was induced only in PPARγ-BATKO mice (Figures 6G and S6F). In general, overexpression of GYK by adenovirus was able to restore the total levels of GYK to approximately 50% of the WT control, and we observed a similar increase of about 40% for total UCP1 levels. These data demonstrate that GYK can modulate iBAT activity *in vivo* and that the effect of PPARγ ablation on UCP1 expression is in part mediated through GYK. Similar to the results obtained from PPARγ knockdown, the respiration of IBAs upon GYK siRNA-mediated knockdown were not changed (Figures 6H and 6I); however, when stimulated by isoproterenol, *Gyk* siRNA-treated cells showed reduced leak respiration. Interestingly, we observed a slight increase in ATP production in *Gyk* siRNA-treated cells under basal condition (Figures 6H and 6I), and a glucose stress test showed that IBAs, upon GYK siRNA knockdown, exhibit an increase in glycolysis (Figures 6J and 6K). GYK generates glycerol-3-phosphate (G3P) from glycerol (Robinson and Newsholme, 1969), which is required to form lysophosphatidic acid (LPA) a key intermediate in TAG

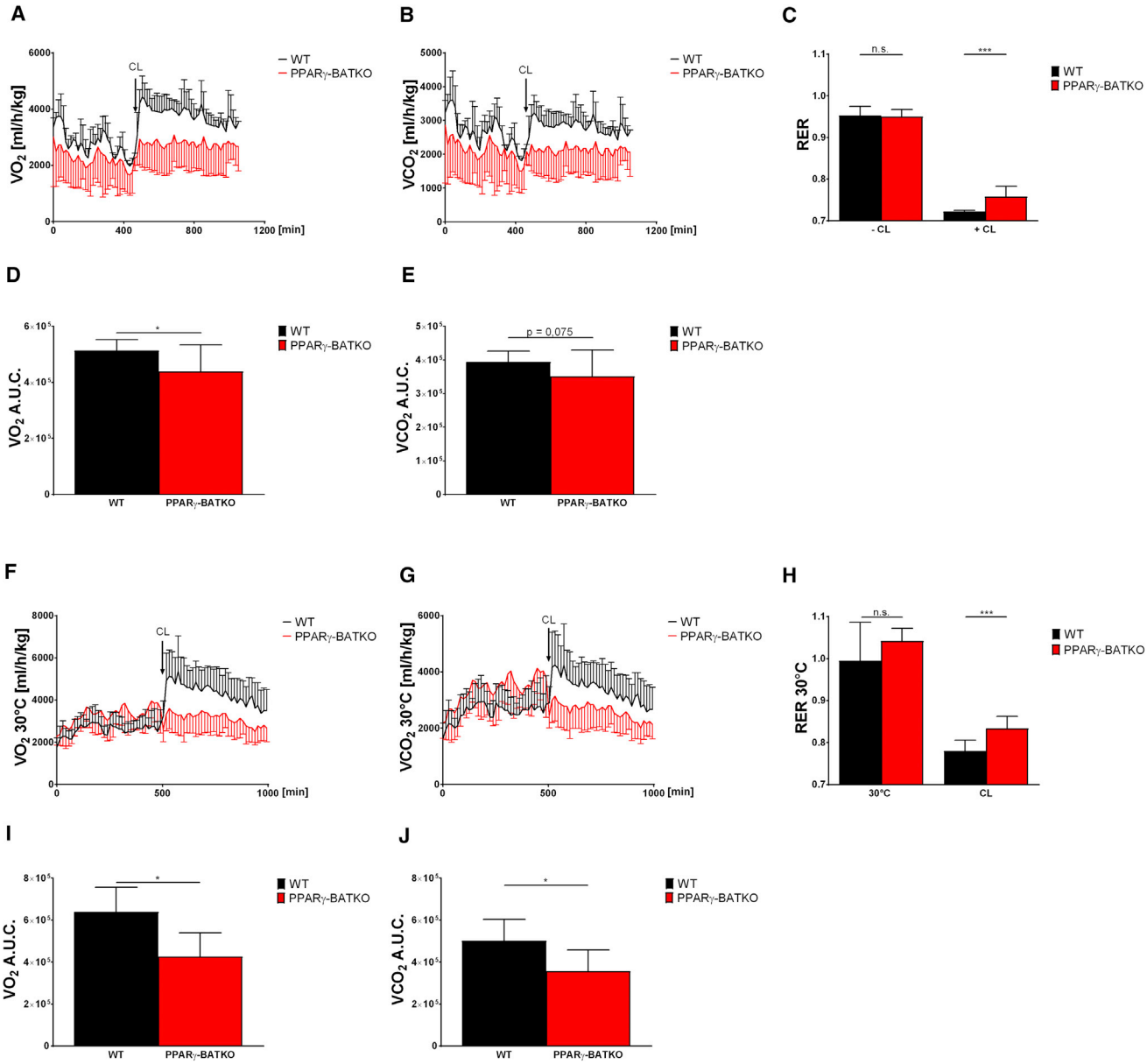


**Figure 3. Lack of PPARγ in BAT Leads to a Reduced Response to Acute β3-Adrenergic Signaling**

(A) $VO_2$ at room temperature (RT) of WT and PPARγ-BATKO with CL316,243 injection (1 mg/kg BM, i.p.) (n = 6 per group).

(B) $VCO_2$ at RT of WT and PPARγ-BATKO with or without CL316,243 injection (1 mg/kg BM, i.p.) (n = 6 per group).

(C) RER of 4 hr before and after CL316,243 injection of WT and PPARγ-BATKO at RT (n = 6 WT versus 6 PPARγ-BATKO; data are expressed as mean ± SD; ***$p \leq 0.005$).

(D) AUC analysis of $VO_2$ at RT of WT and PPARγ-BATKO after CL316,243 (CL) injection (n = 6 WT versus 6 PPARγ-BATKO; data are expressed as mean ± SD; *$p \leq 0.05$).

(E) AUC analysis of $VCO_2$ at RT of WT and PPARγ-BATKO after CL injection (n = 6 WT versus 6 PPARγ-BATKO; data are expressed as mean ± SD).

(F) $VO_2$ of WT and PPARγ-BATKO with CL316,243 injection (1 mg/kg BM, i.p.) at 30°C (n = 6 per group).

(G) $VCO_2$ of WT and PPARγ-BATKO with or without CL316,243 injection (1 mg/kg BM, i.p.) at 30°C (n = 6 per group).

(H) RER of 4 hr before and 4 hr after CL316,243 injection of WT and PPARγ-BATKO at 30°C (n = 6 WT versus 6 PPARγ-BATKO; data are expressed as mean ± SD; ***$p \leq 0.005$).

(I) AUC analysis of $VO_2$ 4 hr after CL316,243 injection of WT and PPARγ-BATKO (n = 6 WT versus 6 PPARγ-BATKO; data are expressed as mean ± SD; *$p \leq 0.05$).

(J) AUC analysis of $VCO_2$ 4 hr after CL316,243 injection of WT and PPARγ-BATKO (n = 6 WT versus 6 PPARγ-BATKO; data are expressed as mean ± SD; *$p \leq 0.05$).

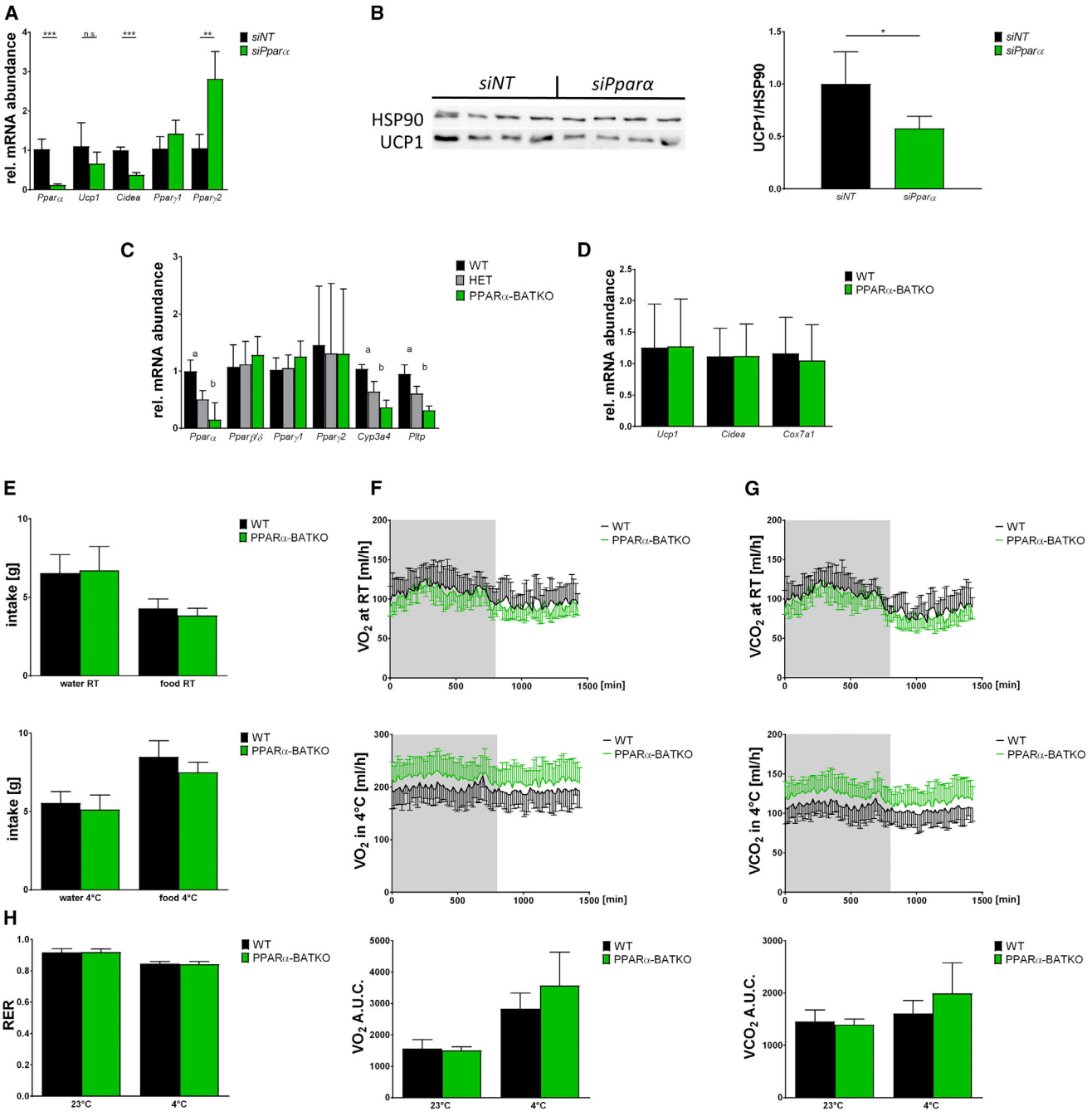


**Figure 4. Loss of PPARα Affects Mature Brown Adipocytes *In Vitro* but Not *In Vivo***

(A) mRNA abundance of reverse transfected IBA with non-targeting (*siNT*) or *Pparα* targeting (*siPPARa*) siRNA showing *Pparα*, *Ucp1*, *Cidea*, *Pparγ1*, and *Pparγ2* normalized to *36B4* (n = 4 per group; data are expressed as mean ± SD; ** $p \leq 0.01$, ***$p \leq 0.005$).

(B) Immunoblot of reverse transfected IBA with siNT and siPPARα and the densiometric analysis of UCP1 to HSP90 (n = 4 per group; data are expressed as mean ± SD; *$p \leq 0.05$).

(C) mRNA abundance of *Pparα*, *Pparβ/δ*, *Pparγ1, Pparγ2, Cyp3a4*, and *Pltp* in BAT of WT, HET, and PPARα-BATKO animals (n = 8 WT versus 7 HET versus 8 PPARα-BATKO).

(D) BAT marker mRNA abundance showing *Ucp1*, *Cidea*, and *Cox7a1* (n = 8 WT versus 7 HET versus 8 PPARα-BATKO).

(E) Water and food intake of 24 hr in RT and in 4°C of WT and PPARα-BATKO (n = 8 WT versus 7 PPARα-BATKO).

(F) $VO_2$ in dark (gray background) and light phase each 12 hr at RT and 4°C of WT and PPARα-BATKO animals as well as AUC analysis (n = 8 WT versus 7 PPARα-BATKO).

*(legend continued on next page)*

synthesis. As expected, both GYK and PPARγ knockdown led to a reduction of G3P in IBAs (Figure 6L) and GYK knockdown led to a reduction of LPA and DAG levels (Figure 6M). Interestingly, fatty acid CoA levels were higher in GYK-ablated cells, suggesting that loss of PPARγ and GYK leads to a reduced capacity for TAG formation. To identify deregulated pathways, we performed microarray analyses on IBAs with GYK ablation. We could identify 124 downregulated and 142 upregulated genes (Tables S4 and S5). Since several of these genes are involved in the regulation of metabolism we performed a transcription factor (TF) enrichment analysis, using the Metacore platform. As shown in Figure 6N the top predicted TFs that could explain the observed regulation were PPARα and PPARγ, suggesting a feedback loop for transcriptional regulation. In conclusion, our data identify the PPARγ/GYK axis as an important node for the maintenance of mature brown function, which is required for inducibility and the capacity to oxidize lipids in response to brown adipocyte activation.

## DISCUSSION

Our results show that PPARγ is necessary to maintain BAT thermogenesis and especially its inducibility by acute thiazolidinediones (TZD), cAMP, or β-adrenergic stimuli in mature brown adipocytes, *in vitro* and *in vivo*. We did not observe any changes in PPARγ and Ucp1 expression in the iWAT depot, which could be due to the timing of the tamoxifen treatment. Since it has been recently shown that the main Ucp1-dependent thermogenic capacity in mice is located in classical BAT we focused our subsequent studies on this particular tissue (Kalinovich et al., 2017). Even though PPARα has an effect on brown adipocyte function *in vitro* (Barbera et al., 2001) and pharmacological activation of PPARα induces brown fat function (van Raalte et al., 2004), we show here that neither PPARα nor PPARβ/δ are required for mature BAT thermogenic functionality, *in vivo*. One possibility for this finding might be that the loss of PPARα can be compensated by PPARγ to regulate brown adipocyte thermogenic function.

Research data from pharmacological studies have identified PPARγ as an important regulator of BAT function. Thus, it is possible to switch in an hMADs cell-culture system the phenotype of a "white like" adipocyte to an activated brown adipocyte even though these cells do not respond to β-adrenergic stimulation. Interestingly, we have recently shown that hMADs cells before rosiglitazone treatment have a protein signature similar to that of a brown adipocyte in the non-activated states (Müller et al., 2016). Therefore, it is possible that pharmacological induction of PPARγ can cause the activation of these cells, although the mechanism is not yet known.

It has been shown that noradrenalin treatment leads to the acute downregulation of PPARγ expression and that its expression is restored after 24 hr, which is in line with our findings presented here (Lindgren et al., 2004). Furthermore, it was reported that mice treated with TZDs induce the amount of BATs, without inducing beta-oxidation. This could be due to negligible effects of brown fat induction, which is unlikely given the strong reported effects of BAT ablation and Ucp1 knock out on the systemic metabolism (Feldmann et al., 2009). A second option is that TZDs promote lipogenesis and dampen the β-adrenergic-mediated activation of adipocytes in vivo, thus masking BAT activation through other systemic alterations. Last, based on the data reported here, it is possible that activation of PPARγ primes the brown adipocytes for induction. This is in line with observations that TZD pre-treatment in cells significantly enhances the inducibility by stimuli such as β-adrenergic activation (Hernandez et al., 2003, 2004).

From the results presented here, we propose that GYK is at least in part required for mediating PPARγ function in BAT and thus constitutes a molecular link for maintenance of inducible brown adipocyte thermogenesis. This is in line with previous reports demonstrating that GYK is a direct PPARγ target in brown adipocytes (Guan et al., 2005). Next to UCP1, several marker genes for brown adipocytes have been reported (Jespersen et al., 2013; Sharp et al., 2012; Ussar et al., 2014). While GYK is not a unique marker for brown tissue our data clearly indicate that GYK is highly correlated with the amount of functional BAT in humans, suggesting that it is required for brown adipocyte thermogenic function. This is supported by the tissue-specific expression of GYK in BAT and liver (Rahib et al., 2007; Robinson and Newsholme, 1967) and the strong induction in WAT over BAT expression coupled to the findings that showed that GYK induction by thiazolidinedione stimulates glycerol incorporation into triglycerides and reduces free fatty acid secretion from adipocytes (Guan et al., 2002).

Based on our data, loss of PPARγ leads to a reduced expression of GYK, thereby reducing the availability of the substrate G3P for esterification of fatty acids, which leads to reduced TAG synthesis and lipid storage. This in turn might lead to a reduced capacity to sustain brown adipocyte function since lipolysis is the main driver of thermogenesis (Haemmerle et al., 2006) and in turn regulates PPARγ activity in BAT. Based on our data, it is furthermore possible that GYK similar to ATGL (Haemmerle et al., 2011) is necessary to maintain the activity of PPARs, which is supported by our observation that the expression of PPARα and PPARγ target genes is reduced in the absence of GYK. Given our data on the role of PPARα in mature brown function, it is plausible that this effect is mainly due to the regulation of PPARγ. Even though multiple different lipids have been suggested as PPARγ ligands it is unlikely that the effect, we observe is ligand dependent, as we were not able to rescue GYK ablation through the addition of rosiglitazone. As it is well established that PPARγ activation is highly dependent on post-transcriptional modifications (Ahmadian et al., 2013), it is possible that GYK knockdown might activate a pathway, which

(G) $VCO_2$ in dark (gray background) and light phase each 12 hr at RT and 4°C of WT and PPARα-BATKO animals as well as AUC analysis (n = 8 WT versus 7 PPARα-BATKO).
(H) RER in RT and 8°C. mRNA data are normalized to *36B4*; data are the mean ± SD. *p < 0.05; ***p < 0.001; not significant (p > 0.05); by one or two-tailed Student's t test.

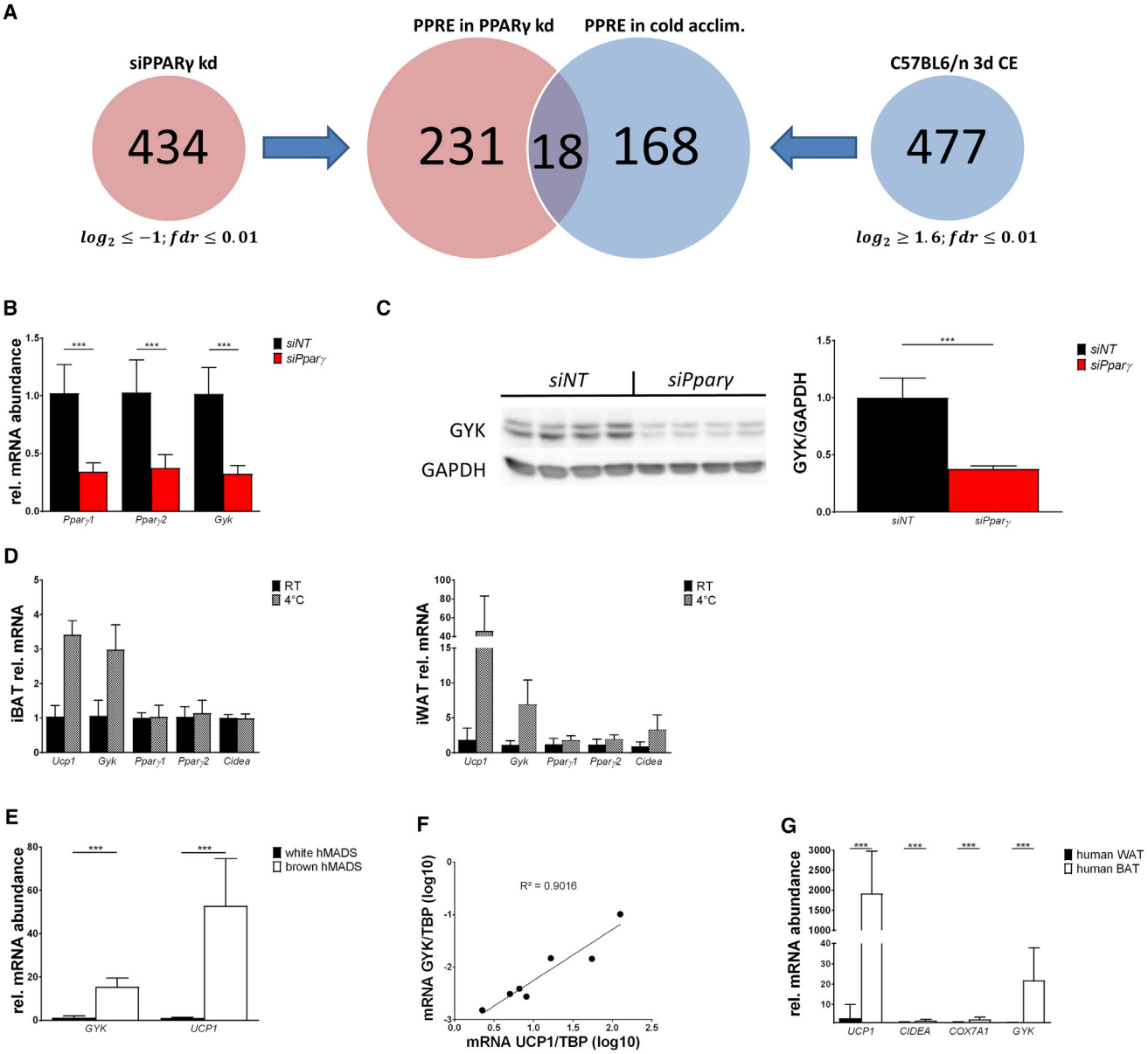


**Figure 5. Gyk Is a Target of PPARγ in Human and Mouse Brown Adipocytes**

(A) Analysis of *Pparγ in vitro* chip microarrays and sequencing data of C57BL6/n in 3-day cold exposure at 8°C.

(B) mRNA abundance of reverse transfected IBA with either *siNT* or *siPPARγ* showing *Pparγ1*, *Pparγ2*, and *Gyk* normalized to *36B4* (n = 4 per group; data are expressed as mean ± SD; ***p ≤ 0.005).

(C) Immunoblot of reverse transfected IBA with either non-targeting (*siNT*) or PPARγ targeting (*siPPARγ*) siRNA showing GYK and its densiometric analysis (n = 4 per group; data are expressed as mean ± SD; ***p ≤ 0.005).

(D)Relative mRNA abundance of *Ucp1* and *Gyk* in BAT and inguinal white adipose tissue (iWAT) of C57BL6/n at RT and 8°C acclimatization for 7 days (n = 5 RT versus 5 8°C).

(E) Relative mRNA abundance of *Ucp1* and *Gyk* of hMADS differentiated into white and brown adipocytes (n = 6 white versus 6 brown; data are expressed as mean ± SD; *p ≤ 0.05).

(F) Correlation of relative mRNA abundance of *UCP1* and *GYK* in human deep-neck samples (n = 7).

(G) Relative mRNA abundance of *UCP1*, *CIDEA*, *COX7A1*, and *GYK* in PET-CT guided human brown and white adipose tissue of the supraclavicular area (n = 7 white versus 7 brown; data are expressed as mean ± SD; ***p ≤ 0.005). mRNA data are normalized to *36B4.*

cause a repression of PPARγ activity, by a so-far unknown post-transcriptional mechanism, independent of ligand-mediated activation.

By overexpressing GYK in interscapular BAT, we could induce thermogenic capacity, similar to an acute cold exposure. Taken together with recent reports demonstrating an induction of

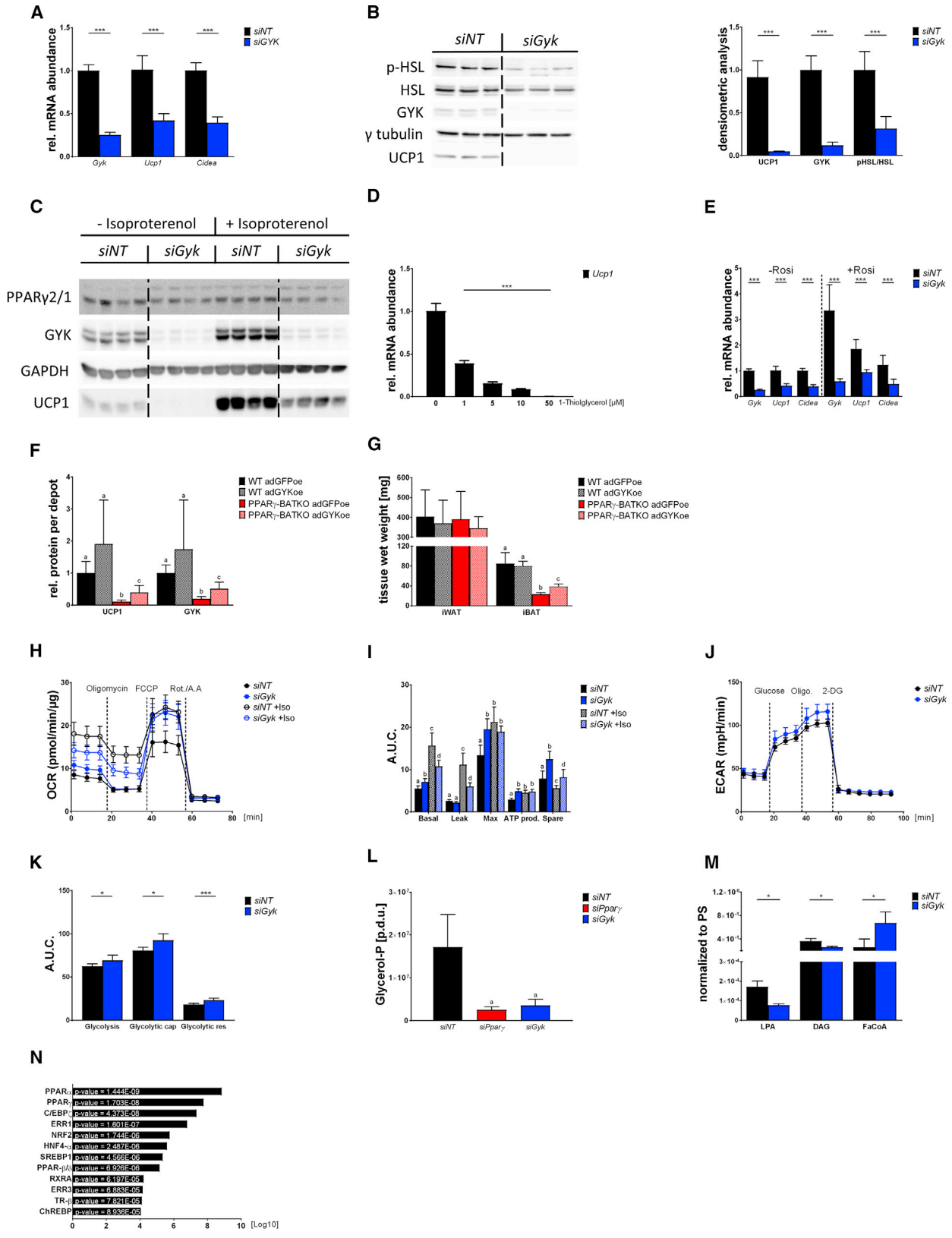


*(legend on next page)*

*Gyk* expression upon cold stimulation (Festuccia et al., 2010; Festuccia et al., 2003), it is likely that GYK mediates cold-induced brown functionality in response to such a stimulus. In this context, our data establish a link between cold induction and PPARγ activation that both induce brown fat functionality. Since TZD-mediated induction of BAT mass and function and β3-receptor activation of thermogenesis are two major regulatory nodes of BAT, our data identify GYK as the link between these two pathways and thus serve as a target for inducing thermogenesis.

## EXPERIMENTAL PROCEDURES

### Mice

C57BL/6N WT mice for experiments and breeding of transgenic lines were obtained from Charles River Laboratories. The mouse strain containing a floxed locus of PPARγ (PPARγfl/fl) was created in the labs of Pierre Chambon (Imai et al., 2004). PPARα and PPARβ/δ animals were provided by W.W. All animals were kept on an inverted 12-hr-light cycle (beginning of dark phase at 7.00 a.m.), fed *ad libitum* chow diet. Animals were kept at 23°C housing temperature when not under cold stimulation. For tissue sampling, animals were euthanized singly in a carbon dioxide atmosphere. Unless stated otherwise, all experiments were performed with adult (11–14 weeks) male mice. Animals used in the study all carried the UCP-ERCre allele (Rosenwald et al., 2013) and the floxed PPAR allele as indicated. Tamoxifen induction of Cre activity was performed as well in WT and knockout (KO) animals by gavaging the mice 4 times with 10 mg/mL per g body mass tamoxifen (Sigma) in sunflower oil (Denner) when kept at 8°C for 6 days. Experiments and further analysis were performed 7 days after cold induction. All animal procedures were approved by national and institutional guidelines.

### Calorimetric Measurements

For measurements of respiratory quotient (respiratory exchange ratio, RER), locomotor activity, food and water intake, a metabolic cage system was used (Phenomaster, TSE Systems). Standard settings according to the manufacturer's instructions were used. Mice were fed *ad libitum* chow diet and water and consumption was determined during a full 24-hr-light cycle after the animals could acclimatize to the cage and/or temperature for 24 hr. Parameters were calculated to individual lean mass that were determined by echo MRI. To generate $\beta_3$-adrenergic stimulation, mice were intraperitoneally (i.p.) injected with CL316,243 1 mg/kg BM.

### Blood Parameters

Whole blood was sampled and adjusted to approximately 5 mM EDTA. Samples were incubated for 10 min at RT and centrifuged 5 min 300 × *g*. Supernatant was flash-frozen in liquid nitrogen. Free fatty acid concentration was determined with the NEFA-HR kit (Wako). To estimate triacylglycerol and cholesterol concentration, Trig/GB and Chol kits (both Roche) were. Blood glucose levels were determined using Contour glucometers (Bayer).

### Glucose Uptake

In IBAs, glucose uptake was performed on the second day after reverse transfection with either non-targeting (NT) siRNA or *Pparγ* siRNA. Cells were incubated at 37°C in Krebs Ringer buffer containing insulin, 2 mM glucose, and C-deoxyglucose (200 cpm/mL). After 2 hr, cells were washed twice with ice-cold PBS and lysed by one freeze thaw cycle in 2 M NaOH. Lysates were mixed with 3 mL scintillation cocktail and intracellular radioactivity was quantified in disintegrations per minute (dpm).

### Paraffin Sections

Adipose tissues were excised, placed in embedding cassettes, and stored in cold PBS. Samples were fixated in 4% paraformaldehyde (Sigma) in PBS (Gibco) at RT. Processing was performed according to the standard protocol in a STP 120 (Microm), and samples were embedded in paraffin and cut into 5-μm-thin sections on a Hyrax M55 (Zeiss). Sections were de-paraffinized and stained with H&E on a Varistain 24-4 (Shandon) before mounting and drying. Images were obtained with an Axioscope A.1 (Zeiss).

### Cell Lines

Immortalized preadipocyte cell lines derived from the stromal-vascular fraction of either interscapular BAT tissue of newborn or young mice were established and provided by Dr. N. Perwitz and Prof. J. Klein (Universität Lübeck) according to standard protocols (Klein et al., 2002; Perwitz et al., 2010). Cells were cultured in high glucose (5 mM) DMEM containing 20% fetal calf serum (FCS). All lines were maintained below confluency. To induce adipogenic differentiation, the cell lines were grown to confluence on collagen-coated tissue culture plates and maintained for 2 additional days. Immortalized brown preadipocytes were induced by stimulation with 115 μg/mL IBMX, 1 μM dexamethasone, 20 nM insulin, 125 μM indomethacin, and 1 nM $T_3$ in full medium. After 24 hr, the medium was exchanged for full medium plus 20 nM insulin and 1 nM $T_3$. Cells were maintained in this medium until sampling for analysis. To stimulate UCP1 expression for final read-out, the cells were incubated in full medium with 1 μM isoproterenol for 8 hr before fixation or lysis.

For siRNA-mediated knockdown, Dharmacon smartPOOL on-target PLUS RNA pools were used for reverse transfection. 25 nmol of siRNA were incubated for 20 min in 0.25% Lipofectamine RNAiMAX in OptiMEM. Subsequently, they were mixed with cells in full growth medium and plated on collagen-coated plates. siRNA-containing medium was replaced by full growth medium 24 hr after lipofection. The sequences of the used siRNAs are listed in Table S3.

**Figure 6. Gyk Is Involved in the Regulation of Brown Adipocyte Inducibility by PPARγ**

(A) mRNA abundance of reverse transfected IBA with siNT and glycerol kinase (siGYK) targeting siRNA showing *Gyk*, *Ucp1*, and *Cidea* normalized to *36B4* (n = 4 per group).

(B) Representative immunoblot of IBA with *siNT* or *siGYK* showing HSL, phosphorylated HSL, GYK, and UCP1, and densiometric quantification (n = 4 per group).

(C) Immunoblot of IBA with *siNT* or *siGyk* with or without isoproterenol (1 mM) (n = 4 per group).

(D) mRNA abundance of *Ucp1* of IBA treated with 1-thiolglycerol at depicted concentrations (n = 4 per group).

(E) mRNA abundance of reverse transfected IBA with *siNT* and *siGyk* with or without rosiglitazone (1 μM) normalized to *36B4* (n = 8 per group).

(F and G) Relative UCP1 protein and GYK abundance in (F) iBAT and (G) tissue wet weight of iWAT and iBAT of WT or PPARγ-BATKO animals 10 days after local adenoviral application into BAT with a $1 \times 10^7$ plaque-forming unit (PFU) adGFP or adGYK adenovirus (n = 4 WT adGFPoe versus 5 WT adGYKoe versus 6 PPARγ-BATKO adGFP versus 7 PPARγ-BATKO adGYKoe. Data are expressed as mean ± SD; a, b, c $p \leq 0.05$).

(H) OCR ratio of IBA *siNT* and *siGYK* from non- to isoproterenol (1 μM) stimulated (OCR-Data normalized to protein content per well; n = 5).

(I) Quantification of mitochondrial stress test (n = 5; data are expressed as mean ± SD; a, b, c, d $\leq 0.05$).

(J) Glucose stress test measurement, showing extracellular acidification rate (ECAR) of IBA *siNT* and *siGyk* ± isoproterenol (1 μM).

(K) Respective quantification of Seahorse glucose stress test (n = 5; data are expressed as mean ± SD; *$p \leq 0.05$; **$p \leq 0.01$; ***$p \leq 0.005$).

(L) Measurement of glycerol-phosphates (Glycerol-P) in IBA treated either with *siNT*, *siPparγ*, or *siGyk* (n = 5–6 per group).

(M) Lysophosphatidic acid (LPA), diacylglycerol (DAG), and fatty acid coenzyme A (FaCoA), normalized to phosphatidylserine (PS) of IBA treated with either *siNT* or *siGyk* (n = 3 per group).

(N) TF enrichment analysis on microarray data from mock transfected iBAs versus iBAs after GYK ablation. Data are expressed as mean ± SD; a and b $p \leq 0.05$). Metacore TF enrichment analysis of *siGyk* knockdown in IBA versus *siNT* controls (p values are annotated; bars depict the inverted p value log to 10).

### hMADS Cell Culture

The establishment and characterization of hMADS cells have been previously described (Rodriguez et al., 2004). Cells were used between passages 14 and 25. Cells were seeded at a density of 5,000 cells/cm$^2$ in DMEM supplemented with 10% FBS, 15 mM HEPES, 2.5 ng/mL hFGF2, 60 mg/mL penicillin, and 50 mg/mL streptomycin. hFGF2 was removed when cells reached confluence. Cells were induced to differentiate at day 2 post-confluence (designated as day 0) in DMEM/Ham's F12 media supplemented with 10 μg/mL transferrin, 10 nM insulin, 0.2 nM triiodothyronine, 1 μm dexamethasone, and 500 μm isobutyl-methylxanthine (IBMX). Two days later, the medium was changed (dexamethasone and IBMX omitted) and 100 nM rosiglitazone was added. At day 9, rosiglitazone was withdrawn to enable white adipocyte differentiation but again included between days 14 and 18 to promote white to brite adipocyte conversion as we previously described (Pisani et al., 2014). Media were changed every other day and cells were used for analyses at day 18.

### White BAT Biopsies from Patients

The clinical study for deep-neck biopsy was approved by the Local Ethics Committee at the University Hospital in Bratislava, Slovakia, and it conforms to the ethical guidelines of the 2000 Helsinki declaration. All study participants provided witnessed written informed consent prior entering the study. Deep-neck and adjacent subcutaneous adipose tissue samples were obtained from the lower third of the neck by an experienced ear, nose, and throat (ENT) surgeon from seven middle-aged (38.7 ± 3.1 years) non-obese (BMI 23.7 ± 0.4 kg/m$^2$; waist circumference 82.1 ± 3.0 cm; body fat 28.7% ± 1.3 %) individuals (1M/6F) during neck surgery under general anesthesia (i.e., thyroid surgery [n = 6] or branchial cleft cyst surgery [n = 1]). The deep-neck adipose tissue sample was taken from pre- and paravertebral space between common carotid and trachea in case of thyroid surgery and just laterally to carotid sheath in case of branchial cleft cyst surgery. In all cases, surgical approach was sufficient to reach and sample the deep-neck adipose tissue without any additional morbidity. Patients with malignant disease and subjects younger than 18 years were excluded from participation in the study. The PET/CT-guided human supraclavicular WAT and BAT samples were taken as previously described (Orava et al., 2011).

### Cellular Respiration

Differentiated cells were reverse transfected on rat collagen-coated 96-well Seahorse cell-culture microplates. The oxygen consumption rate (OCR) measurements were performed at 37°C using an XF96 extracellular flux analyzer (Seahorse Bioscience).

### RNA Extraction, cDNA Synthesis, and Quantitative Real-Time PCR

Total RNA was extracted from tissues or unsorted cells using Trizol reagent (Invitrogen). Final RNA samples were re-precipitated with NaOAc and ethanol and washed with 70% ethanol before analysis on a Nanodrop-2000 spectrophotometer. RNA from the human supraclavicular WAT and BAT samples was isolated as previously described (Orava et al., 2011). Reverse transcription was performed using the High Capacity cDNA Reverse transcription kit (Applied Biosystems) with 20–2,000 ng of RNA for cell preparations or whole-tissue preparations. qPCR was performed on a StepOnePlus (Applied Biosystems), and relative mRNA concentrations normalized to the expression of 36B4 were calculated by the ΔΔCt method. qPCR primers and TaqMan probes are listed in Table S2.

### Microarrays

For microarray analyses, RNA preparations were checked for RNA integrity and purity on Bioanalyser RNA nano chips. In case of adipocyte or SVF preparations, 600 ng of total RNA per sample was labeled with the Microarray Quick Amp Labelling Kit (Agilent) according to the manufacturer's instructions. RNA samples of whole adipose tissue were labeled as a service provided by the Functional Genomics Centre Zurich (FGCZ). Hybridization to 4 × 44k whole-mouse microarrays (Agilent) measurements and processing of raw data were provided by the FGCZ. TF enrichment analysis was performed using the Metacore platform.

### Western Blotting

Protein amounts were assessed using the DC Protein Assay (Bio-Rad). Western blotting was carried out following standard procedures and chemiluminescence signals were detected by an LAS 4000 mini ImageQuant system (GE Healthcare). Primary antibodies used were as follows: UCP1 (1:1,000; ab10983 Abcam), HSL (1:1,000; #4107 Cell Signaling Technology), p-HSL (Ser660, 1:1,000; #4126 Cell Signal), GAPDH (D16H11, 1:1,000; #5174 Cell Signal), γ-tubulin (1:1,000; T6557 Sigma), p-CREB (S133, 1:1000; #9198 Cell Signal), CREB (1:1,000; #9197 Cell Signal), S6 ribosomal Protein (1:1,000; #2217 Cell Signal), p-S6 ribosomal Protein (1:1,000; #5364 Cell Signal), PPARγ (1:1,000; #2443 Cell Signal), GYK (1:1,000; ab126599 Abcam), and HSP90 (1:1,000; #4877 Cell Signal).

### Metabolomics

IBAs were reverse transected in a 6-well plate with approximately 5 × 105 cells/well. Cells were left to attach for approximately 24 hr, followed by complete medium removal, and washed with 1 × PBS. Fresh medium was added, and cells were incubated for further 24 hr. Sampling for metabolomics experiment was performed as follows: the medium was removed, and cells were washed twice with cold PBS and quenched by snap freezing the plate in liquid N2. Plates were stored at –80°C until proceeding with metabolite extraction. The cold (–20°C) extraction solution (acetonitrile/methanol/water [2:2:1]) was used for metabolite extraction. 400 μL of cold extraction solution was added to each well and incubated for 10 min at –20°C. The supernatant was transferred to a tube and stored on ice. Then, the extraction was repeated by adding additionally 400 μL of cold extraction solution followed by an incubation at –20°C. By keeping the plates on ice, cells were scraped and transferred to the same tube used for the first extraction. Extracts were centrifuged (4°C, 13,000 rpm for 2 min), and the supernatants were transferred to fresh tubes. Clean extracts were used for untargeted metabolomics, while supernatants were evaporated to complete dryness for targeted measurements. For targeted metabolomics, the dried samples were resuspended in 100 μL deionized water, and 15-μL aliquots were injected into a Waters Acquity UPLC (Waters Corporation, Milford, MA) with a Waters Acquity T3 column coupled to a Thermo TSQ Quantum Ultra triple quadrupole instrument (Thermo Fisher Scientific) with negative-mode electrospray ionization. Compounds were separated by a gradient of two mobile phases (A) 10 mM tributylamine, 15 mM acetic acid and 5% (v/v) methanol, and (B) 2-propanol. Acquisition of mass isotopomer distributions of intact and fragmented carbon backbones was done as previously described (Rühl et al., 2012).

### Statistical Analysis

Unless stated otherwise, data are presented as mean ± SD. Unpaired and paired two-sided Student's t tests were used for comparisons with $^*p < 0.05$, $^{**}p < 0.01$, and $^{***}p < 0.005$ compared with control group. $p > 0.05$ are marked as not significant or depicted with their exact p value. Area under the curve (AUC) was calculated using the trapezoid method. Metabolomics data were analyzed by using MATLAB R2015b and software developed in house. Student's t test distribution was used for calculating the significant changing metabolites between different groups. Storey's multiple testing correction was used for p values to account for false discovery rate (Storey and Tibshirani, 2003).

## DATA AND SOFTWARE AVAILABILITY

The accession number for the microarray data in this study is NCBI GEO: GSE103474.

## SUPPLEMENTAL INFORMATION

Supplemental Information includes six figures and five tables and can be found with this article online at https://doi.org/10.1016/j.celrep.2017.12.067.

## ACKNOWLEDGMENTS

This study received financial support from the Swiss National Foundation (SNF), grant number 31003A_162887 (C.W.). W.W. is supported by a start-up

grant from Lee Kong Chian School of Medicine and Nanyang Technological University, Singapore. M.E.L. is supported by the Swedish Research Council (2013–4466). S.E. is supported by the Swedish Research Council (2012–1652, 2014–2516).

## AUTHOR CONTRIBUTIONS

D.L., M.R., and C.W. designed the study, and D.L. and C.W. wrote the paper. D.L. performed most of the experiments; E.K. and W.S. performed FFA uptake, FFA release, glucose uptake *in vitro*, and histological sections of PPARγ-BATKO with cell density analysis; M.R. performed PPARγ-BATKO food and water intake and body mass development and determined blood triglyceride, cholesterol, NEFA, and glucose level measurement, PPARα food and water intake, and indirect calorimetry analysis in those mice; B.T. cloned the adenovirus for Gyk overexpression; L.O. analyzed the microarrays; L.V., P.S., and J.U. obtained the human biopsies; M.B. processed human samples; W.W. provided the PPARα fl/fl and PPARβ/δ fl/fl mice; E.-Z.A. provided the human brown cell line; and P.K. and N.Z. performed untargeted and targets metabolomics. M.E.L., P.N., and K.V. processed human samples and critically reviewed the paper. S.E. took part in designing experiments and critically reviewed the paper.

## DECLARATION OF INTERESTS

The authors declare no competing interests.

Received: July 10, 2017
Revised: October 3, 2017
Accepted: December 20, 2017
Published: January 16, 2018

## REFERENCES

Ahmadian, M., Suh, J.M., Hah, N., Liddle, C., Atkins, A.R., Downes, M., and Evans, R.M. (2013). PPARγ signaling and metabolism: The good, the bad and the future. Nat. Med. *19*, 557–566.

Barak, Y., Nelson, M.C., Ong, E.S., Jones, Y.Z., Ruiz-Lozano, P., Chien, K.R., Koder, A., and Evans, R.M. (1999). PPAR gamma is required for placental, cardiac, and adipose tissue development. Mol. Cell *4*, 585–595.

Barbera, M.J., Schluter, A., Pedraza, N., Iglesias, R., Villarroya, F., and Giralt, M. (2001). Peroxisome proliferator-activated receptor alpha activates transcription of the brown fat uncoupling protein-1 gene. A link between regulation of the thermogenic and lipid oxidation pathways in the brown fat cell. J. Biol. Chem. *276*, 1486–1493.

Barquissau, V., Beuzelin, D., Pisani, D.F., Beranger, G.E., Mairal, A., Montagner, A., Roussel, B., Tavernier, G., Marques, M.A., Moro, C., et al. (2016). White-to-brite conversion in human adipocytes promotes metabolic reprogramming towards fatty acid anabolic and catabolic pathways. Mol. Metab. *5*, 352–365.

Cao, W., Daniel, K.W., Robidoux, J., Puigserver, P., Medvedev, A.V., Bai, X., Floering, L.M., Spiegelman, B.M., and Collins, S. (2004). p38 mitogen-activated protein kinase is the central regulator of cyclic AMP-dependent transcription of the brown fat uncoupling protein 1 gene. Mol. Cell. Biol. *24*, 3057–3067.

Chakrabarty, K., Chaudhuri, B., and Jeffay, H. (1983). Glycerokinase activity in human brown adipose tissue. J. Lipid Res. *24*, 381–390.

Choi, J.H., Banks, A.S., Estall, J.L., Kajimura, S., Boström, P., Laznik, D., Ruas, J.L., Chalmers, M.J., Kamenecka, T.M., Blüher, M., et al. (2010). Anti-diabetic drugs inhibit obesity-linked phosphorylation of PPARgamma by Cdk5. Nature *466*, 451–456.

Feldmann, H.M., Golozoubova, V., Cannon, B., and Nedergaard, J. (2009). UCP1 ablation induces obesity and abolishes diet-induced thermogenesis in mice exempt from thermal stress by living at thermoneutrality. Cell Metab. *9*, 203–209.

Festuccia, W.T., Guerra-Sá, R., Kawashita, N.H., Garófalo, M.A., Evangelista, E.A., Rodrigues, V., Kettelhut, I.C., and Migliorini, R.H. (2003). Expression of glycerokinase in brown adipose tissue is stimulated by the sympathetic nervous system. Am. J. Physiol. Regul. Integr. Comp. Physiol. *284*, R1536–R1541.

Festuccia, W.T., Blanchard, P.G., Richard, D., and Deshaies, Y. (2010). Basal adrenergic tone is required for maximal stimulation of rat brown adipose tissue UCP1 expression by chronic PPAR-gamma activation. Am. J. Physiol. Regul. Integr. Comp. Physiol. *299*, R159–R167.

Guan, H.P., Li, Y., Jensen, M.V., Newgard, C.B., Steppan, C.M., and Lazar, M.A. (2002). A futile metabolic cycle activated in adipocytes by antidiabetic agents. Nat. Med. *8*, 1122–1128.

Guan, H.P., Ishizuka, T., Chui, P.C., Lehrke, M., and Lazar, M.A. (2005). Corepressors selectively control the transcriptional activity of PPARgamma in adipocytes. Genes Dev. *19*, 453–461.

Haemmerle, G., Lass, A., Zimmermann, R., Gorkiewicz, G., Meyer, C., Rozman, J., Heldmaier, G., Maier, R., Theussl, C., Eder, S., et al. (2006). Defective lipolysis and altered energy metabolism in mice lacking adipose triglyceride lipase. Science *312*, 734–737.

Haemmerle, G., Moustafa, T., Woelkart, G., Büttner, S., Schmidt, A., van de Weijer, T., Hesselink, M., Jaeger, D., Kienesberger, P.C., Zierler, K., et al. (2011). ATGL-mediated fat catabolism regulates cardiac mitochondrial function via PPAR-α and PGC-1. Nat. Med. *17*, 1076–1085.

He, W., Barak, Y., Hevener, A., Olson, P., Liao, D., Le, J., Nelson, M., Ong, E., Olefsky, J.M., and Evans, R.M. (2003). Adipose-specific peroxisome proliferator-activated receptor gamma knockout causes insulin resistance in fat and liver but not in muscle. Proc. Natl. Acad. Sci. USA *100*, 15712–15717.

Hernandez, R., Teruel, T., and Lorenzo, M. (2003). Rosiglitazone produces insulin sensitisation by increasing expression of the insulin receptor and its tyrosine kinase activity in brown adipocytes. Diabetologia *46*, 1618–1628.

Hernandez, R., Teruel, T., de Alvaro, C., and Lorenzo, M. (2004). Rosiglitazone ameliorates insulin resistance in brown adipocytes of Wistar rats by impairing TNF-alpha induction of p38 and p42/p44 mitogen-activated protein kinases. Diabetologia *47*, 1615–1624.

Hill, J.O., Wyatt, H.R., and Peters, J.C. (2012). Energy balance and obesity. Circulation *126*, 126–132.

Hu, E., Kim, J.B., Sarraf, P., and Spiegelman, B.M. (1996). Inhibition of adipogenesis through MAP kinase-mediated phosphorylation of PPARgamma. Science *274*, 2100–2103.

Imai, T., Takakuwa, R., Marchand, S., Dentz, E., Bornert, J.M., Messaddeq, N., Wendling, O., Mark, M., Desvergne, B., Wahli, W., et al. (2004). Peroxisome proliferator-activated receptor gamma is required in mature white and brown adipocytes for their survival in the mouse. Proc. Natl. Acad. Sci. USA *101*, 4543–4547.

Jespersen, N.Z., Larsen, T.J., Peijs, L., Daugaard, S., Homøe, P., Loft, A., de Jong, J., Mathur, N., Cannon, B., Nedergaard, J., et al. (2013). A classical brown adipose tissue mRNA signature partly overlaps with brite in the supraclavicular region of adult humans. Cell Metab. *17*, 798–805.

Jones, J.R., Barrick, C., Kim, K.A., Lindner, J., Blondeau, B., Fujimoto, Y., Shiota, M., Kesterson, R.A., Kahn, B.B., and Magnuson, M.A. (2005). Deletion of PPARgamma in adipose tissues of mice protects against high fat diet-induced obesity and insulin resistance. Proc. Natl. Acad. Sci. USA *102*, 6207–6212.

Kalinovich, A.V., de Jong, J.M., Cannon, B., and Nedergaard, J. (2017). UCP1 in adipose tissues: Two steps to full browning. Biochimie *134*, 127–137.

Klein, J., Fasshauer, M., Klein, H.H., Benito, M., and Kahn, C.R. (2002). Novel adipocyte lines from brown fat: A model system for the study of differentiation, energy metabolism, and insulin action. BioEssays *24*, 382–388.

Lindgren, E.M., Nielsen, R., Petrovic, N., Jacobsson, A., Mandrup, S., Cannon, B., and Nedergaard, J. (2004). Noradrenaline represses PPAR (peroxisome-proliferator-activated receptor) gamma2 gene expression in brown adipocytes: Intracellular signalling and effects on PPARgamma2 and PPARgamma1 protein levels. Biochem. J. *382*, 597–606.

Loft, A., Forss, I., Siersbæk, M.S., Schmidt, S.F., Larsen, A.S., Madsen, J.G., Pisani, D.F., Nielsen, R., Aagaard, M.M., Mathison, A., et al. (2015). Browning of human adipocytes requires KLF11 and reprogramming of PPARγ superenhancers. Genes Dev. *29*, 7–22.

Mazzucotelli, A., Viguerie, N., Tiraby, C., Annicotte, J.S., Mairal, A., Klimcakova, E., Lepin, E., Delmar, P., Dejean, S., Tavernier, G., et al. (2007). The transcriptional coactivator peroxisome proliferator activated receptor (PPAR)gamma coactivator-1 alpha and the nuclear receptor PPAR alpha control the expression of glycerol kinase and metabolism genes independently of PPAR gamma activation in human white adipocytes. Diabetes *56*, 2467–2475.

Mittendorfer, B. (2011). Origins of metabolic complications in obesity: Adipose tissue and free fatty acid trafficking. Curr. Opin. Clin. Nutr. Metab. Care *14*, 535–541.

Müller, S., Balaz, M., Stefanicka, P., Varga, L., Amri, E.Z., Ukropec, J., Wollscheid, B., and Wolfrum, C. (2016). Proteomic analysis of human brown adipose tissue reveals utilization of coupled and uncoupled energy expenditure pathways. Sci. Rep. *6*, 30030.

Nielsen, R., Pedersen, T.A., Hagenbeek, D., Moulos, P., Siersbaek, R., Megens, E., Denissov, S., Børgesen, M., Francoijs, K.J., Mandrup, S., and Stunnenberg, H.G. (2008). Genome-wide profiling of PPARgamma:RXR and RNA polymerase II occupancy reveals temporal activation of distinct metabolic pathways and changes in RXR dimer composition during adipogenesis. Genes Dev. *22*, 2953–2967.

Ohno, H., Shinoda, K., Spiegelman, B.M., and Kajimura, S. (2012). PPARγ agonists induce a white-to-brown fat conversion through stabilization of PRDM16 protein. Cell Metab. *15*, 395–404.

Orava, J., Nuutila, P., Lidell, M.E., Oikonen, V., Noponen, T., Viljanen, T., Scheinin, M., Taittonen, M., Niemi, T., Enerbäck, S., and Virtanen, K.A. (2011). Different metabolic responses of human brown adipose tissue to activation by cold and insulin. Cell Metab. *14*, 272–279.

Perwitz, N., Wenzel, J., Wagner, I., Büning, J., Drenckhan, M., Zarse, K., Ristow, M., Lilienthal, W., Lehnert, H., and Klein, J. (2010). Cannabinoid type 1 receptor blockade induces transdifferentiation towards a brown fat phenotype in white adipocytes. Diabetes Obes. Metab. *12*, 158–166.

Petrovic, N., Walden, T.B., Shabalina, I.G., Timmons, J.A., Cannon, B., and Nedergaard, J. (2010). Chronic peroxisome proliferator-activated receptor gamma (PPARgamma) activation of epididymally derived white adipocyte cultures reveals a population of thermogenically competent, UCP1-containing adipocytes molecularly distinct from classic brown adipocytes. J. Biol. Chem. *285*, 7153–7164.

Pisani, D.F., Ghandour, R.A., Beranger, G.E., Le Faouder, P., Chambard, J.C., Giroud, M., Vegiopoulos, A., Djedaini, M., Bertrand-Michel, J., Tauc, M., et al. (2014). The ω6-fatty acid, arachidonic acid, regulates the conversion of white to brite adipocyte through a prostaglandin/calcium mediated pathway. Mol. Metab. *3*, 834–847.

Qiang, L., Wang, L., Kon, N., Zhao, W., Lee, S., Zhang, Y., Rosenbaum, M., Zhao, Y., Gu, W., Farmer, S.R., and Accili, D. (2012). Brown remodeling of white adipose tissue by SirT1-dependent deacetylation of Pparγ. Cell *150*, 620–632.

Rahib, L., MacLennan, N.K., Horvath, S., Liao, J.C., and Dipple, K.M. (2007). Glycerol kinase deficiency alters expression of genes involved in lipid metabolism, carbohydrate metabolism, and insulin signaling. Eur. J. Hum. Genet. *15*, 646–657.

Robinson, J., and Newsholme, E.A. (1967). Glycerol kinase activities in rat heart and adipose tissue. Biochem. J. *104*, 2C–4C.

Robinson, J., and Newsholme, E.A. (1969). Some properties of hepatic glycerol kinase and their relation to the control of glycerol utilization. Biochem. J. *112*, 455–464.

Rodriguez, A.M., Elabd, C., Delteil, F., Astier, J., Vernochet, C., Saint-Marc, P., Guesnet, J., Guezennec, A., Amri, E.Z., Dani, C., and Ailhaud, G. (2004). Adipocyte differentiation of multipotent cells established from human adipose tissue. Biochem. Biophys. Res. Commun. *315*, 255–263.

Rosenwald, M., Perdikari, A., Rülicke, T., and Wolfrum, C. (2013). Bi-directional interconversion of brite and white adipocytes. Nat. Cell Biol. *15*, 659–667.

Rühl, M., Rupp, B., Nöh, K., Wiechert, W., Sauer, U., and Zamboni, N. (2012). Collisional fragmentation of central carbon metabolites in LC-MS/MS increases precision of $^{13}C$ metabolic flux analysis. Biotechnol. Bioeng. *109*, 763–771.

Seltzer, W.K., Dhariwal, G., Mckelvey, H.A., and McCabe, E.R. (1986). 1-Thioglycerol: Inhibitor of glycerol kinase activity in vitro and in situ. Life Sci. *39*, 1417–1424.

Sharp, L.Z., Shinoda, K., Ohno, H., Scheel, D.W., Tomoda, E., Ruiz, L., Hu, H., Wang, L., Pavlova, Z., Gilsanz, V., and Kajimura, S. (2012). Human BAT possesses molecular signatures that resemble beige/brite cells. PLoS ONE *7*, e49452.

Shefer, V.I., and Talan, M.I. (1998). The effect of exercise training in cold on shivering and nonshivering thermogenesis in adult and aged C57BL/6J mice. Exp. Gerontol. *33*, 467–476.

Storey, J.D., and Tibshirani, R. (2003). Statistical significance for genomewide studies. Proc. Natl. Acad. Sci. USA *100*, 9440–9445.

Tontonoz, P., Hu, E., Graves, R.A., Budavari, A.I., and Spiegelman, B.M. (1994). mPPAR gamma 2: Tissue-specific regulator of an adipocyte enhancer. Genes Dev. *8*, 1224–1234.

Ussar, S., Lee, K.Y., Dankel, S.N., Boucher, J., Haering, M.F., Kleinridders, A., Thomou, T., Xue, R., Macotela, Y., Cypess, A.M., et al. (2014). ASC-1, PAT2, and P2RX5 are cell surface markers for white, beige, and brown adipocytes. Sci. Transl. Med. *6*, 247ra103.

van Raalte, D.H., Li, M., Pritchard, P.H., and Wasan, K.M. (2004). Peroxisome proliferator-activated receptor (PPAR)-alpha: A pharmacological target with a promising future. Pharm. Res. *21*, 1531–1538.